Available online at www.sciencedirect.com
ScienceDirect
Acta Biomaterialia 4 (2008) 2016–2027
Acta BIOMATERIALIA
www.elsevier.com/locate/actabiomat

Effects of intermediate dielectric films on multilayer surface plasmon resonance behavior

Manwen Yao [a,*], Ooi-Kiang Tan [b], Swee-Chuan Tjin [b,c], John C. Wolfe [a]

[a] *Department of Electrical and Computer Engineering, University of Houston, N 308 Engineering Building 1, Houston, TX 77204, USA*
[b] *School of Electrical and Electronic Engineering, Nanyang Technological University, 50 Nanyang Avenue, Singapore 639798, Singapore*
[c] *Singapore-University of Washington Alliance (SUWA), 50 Nanyang Avenue, Singapore 639798, Singapore*

Received 2 August 2007; received in revised form 28 May 2008; accepted 13 June 2008
Available online 25 June 2008

Abstract

The effects of intermediate dielectric films on multilayer surface plasmon resonance (SPR) behavior were studied in terms of biosensing applications. Ten simple and complex oxides and fluoride, including MgF_2 and MgO, SiO_2, TiO_2 and complex PZT family dielectric materials, were evaluated. The materials cover a wide range of refractive indices, from 1.19 for the porous silica film to 2.83 for the TiO_2 film. The resonance curves of the multilayer SPR configurations were taken from an angular modulated Kretschmann set-up under a fixed incident wavelength of 543.5 nm. The intermediate dielectric layer has no strong effect on the SPR resonance angle and minimum reflectance at the resonance point. Some intermediate dielectric films, such as MgF_2, porous silica, TiO_2 and PLZT, apparently reduce the width of the resonance curves, resulting in sharper resonance dips. Better performance of the multilayer SPR biosensor incorporating these dielectric films is expected.
Published by Elsevier Ltd. on behalf of Acta Materialia Inc.

Keywords: Surface plasmon resonance; Biosensing; Multilayer configuration; Dielectric thin film

1. Introduction

Surface plasmon resonance (SPR) was first introduced into biosensors by Nylander and Liedberg in 1982 [1–3]. Since then, many works have been devoted to the development of SPR-based biological sensing. Among a wealth of biosensing techniques, SPR has been recognized as a valuable and standard analytical tool in biophysical and biochemical studies. The technique offers several distinctive features, such as high sensitivity, label-free measurement and real time analysis [4].

Surface plasmon waves (SPWs) can be easily excited at the interface between two media with dielectric constants of opposite signs, such as a metal and a dielectric, by an incident electromagnetic light wave. This SPW is confined to a very narrow range of a few nanometers within the metal surface, while it penetrates tens or hundreds nanometers into the dielectric medium. Surface waves within both the metal and the dielectric evanesce away from the interface. The electric field of the SPW at the interface is very strong and much enhanced in orders of magnitude. Consequently, the SPR technique is very sensitive to environmental changes in the close vicinity of the interface. Any changes in the chemical composition of the environment that occur at the metal–dielectric interface can be monitored by the SPR measurement. This allows the detection of any pair of molecules that exhibits specific binding, which could be an antigen and antibody, a DNA probe and complementary DNA strand, or an enzyme and its substrate [5–13].

The SPW arises from the energy transfer from the incident light wave (quantified as photon) into an electron charge density wave or SPW (quantified as plasmon) at the surface of a solid which has a free electron-like structure. When the energy of the light is coupled into the metal's surface, collective resonance of electrons can be

* Corresponding author. Tel.: +1 713 743 4481.
E-mail address: myao@mail.uh.edu (M. Yao).

1742-7061/$ - see front matter Published by Elsevier Ltd. on behalf of Acta Materialia Inc.
doi:10.1016/j.actbio.2008.06.002

generated. The energy transfer from photon to plasmon is regarded as surface plasmon resonance (SPR) [14,15].

The most widely used method to excite SPR is known as Kretschmann prism-coupler-based SPR, in which the incident light passes through an optically dense medium, usually a prism, to match the wave vector of the SPW. The metal film is deposited directly onto the prism surface [16]. The surface plasmons are excited at the metal/air interface. Since the surface plasmon is transverse magnetic (TM), SPR has to be excited by a light beam with *p*-polarization (TM mode). The resonant condition is tuned by either varying the angle of the incident light at fixed wavelength or varying the wavelength of the incident light at fixed incident angle; these are referred to as angular modulation and wavelength modulation, respectively [14]. When the resonant condition is satisfied, a sharp decrease in reflectivity occurs where the energy of incident light is almost completely absorbed and transferred from photon to plasmon. The resulting dip in reflectance R vs. light incident angle θ is often referred to as the SPR curve.

The SPR curve is usually characterized by three major features: the resonant angle θ_R, the minimum reflectance or resonant depth R_{min} and the width of the resonant curve $\Delta\theta$ [17,18]. In biosensor applications of the prism-coupler-based SPR, the analyte under test is placed on the metal interface performing as the second medium of the prism/metal/analyte configuration. Any changes in refractive index or thickness of the analyte result in changes of the wave vector of the SPW, hence the changes of the resonance curve features. From these changes, the changes of the analyte can be elicited. All the features of the SPR curve are dependent on the incident wavelength, dielectric constant and thickness of metal film, and the refractive index of the prism as well as the analyte [14]. There are many ways to modulate the resonant condition by various combinations of the above factors in a SPR configuration. To achieve better performances of the SPR sensor, optimized combinations of SPR configuration should be developed from case to case.

The technology of SPR biosensors based on the conventional Kretschmann configuration has been well developed. All kinds of means to improve its performances have been widely studied. The achievements of all these studies have been adapted and integrated into commercialized SPR systems. It has been said that there is not much room for further improvement in traditional SPR sensors. Therefore other development strategies and new approaches have to be explored.

One recent effort is the application of the multiple-phase Kretschmann configuration, in which an intermediate dielectric layer is intercalated between the prism and the metal film, as shown in Fig. 1. It has been confirmed that the introduction of an intermediate dielectric layer results in much larger propagation lengths of SPW along and perpendicular to the interface because the electric field of SPW is significantly redistributed across the multilayer structure, with a large fraction of the electric field existing in the less low loss intermediate dielectric layer; while for its counterpart, the conventional SPW decays rapidly within the high loss metal. Consequently, the multilayer SPR would exhibit a sharper resonance curve with a narrower resonance width in comparison with the conventional SPR [19,20].

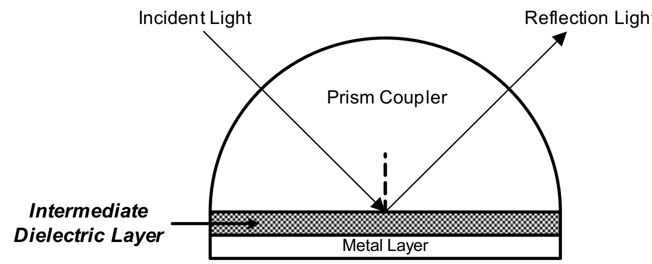

Fig. 1. Schematic of multilayer SPR.

In general, in any measuring system utilizing the resonance phenomenon, a sharper resonance behavior means a greater sensitivity and a better resolution of the measurement. In the case of SPR biosensing, a sharper SPR curve (a narrower band width) would definitely result in greater sensitivity and finer resolution. The exact relation between the two factors is rather complicated. The sensitivity of a SPR biosensing system is a colligated parameter relating to many aspects of the measurements, such as the characteristics of the system (resolution, noise level, etc.), the measuring mode (measurants, fixed or variable angular mode, fixed or variable wavelength mode, etc.), and physical and biological aspects of the analyte samples (gaseous or liquids, film or bulk, etc.). It should be ideally investigated from case to case, but here we used the width of the resonance curve as a criterion to compare various SPR configurations.

The widths of the SPR curves, as discussed above, are affected by many factors. The dielectric constant and thickness of the metal film have very strong effects on the features of the resonant curve. It is widely recognized that silver (Ag) results in the sharpest resonance curve [21]. The wavelength of the incident light also has a strong effect on the resonant characteristics. A longer wavelength results in a lower resonant angle and a sharper resonant curve. Brink et al. [22] suggested that working in the near-infrared range would result in greater sensitivity.

The refractive index of the prism also affects the resonant behavior. Our experimental results and computer simulation revealed that a higher refractive index of the prism results in a lower resonance angle and a sharper resonant curve. To obtain a high-performance SPR biosensor, the above three factors should all be taken into account. Ideally, an SPR set-up using a prism with high refractive index coated with a reasonable thickness of silver working under a near-infrared wavelength would deliver the sharpest resonant curve and highest performance. However, there are many practical restrictions. For example, most SPR systems use gold film instead of silver because of the high chemical inertia and very good bioaffinity of the gold film.

In this light, we were trying to explore alternative ways to improve the sensing performance of the SPR system further. Hopefully the findings from this study of an intermediate dielectric film in a multilayer SPR can be adopted in various optimized SPR configurations and so improve their performance. We are not trying to propose an optimized SPR plot. Therefore, we worked on a common prism-coupler-based SPR configuration working under a fixed wavelength as our model system to reveal the effect of the intermediate dielectric film.

In this study, with an SPR system working under a fixed incident wavelength for the purpose of biosensing, a figure of merit $Q = \theta_R/\Delta\theta$ can be used to characterize the performance of the system with various configurations, where θ_R is the resonance angle and $\Delta\theta$ is the width of the resonant curve. The lower the resonant width $\Delta\theta$, the higher the figure of the merit Q and the higher the sensitivity and resolution of the system that can be achieved [21,23].

It should be noted that in the multilayer SPR geometry the SPW is extended much further into the sample medium attached to the sensing surface of the metal film due to a greater penetration depth of the electromagnetic field, which means much more field intensity is located in the volume of analyte to be tested. As a result, the sensitivity in the monitoring of a bio-binding event can be improved and the fluctuation of the measurement can be effectively suppressed. This is especially significant for the detection of large bacterial cells (usually 1 μm in diameter), because these may remain outside the volume that can be probed with conventional surface plasmon measurement.

Few studies have focused on multilayer SPR-based biosensors. The theoretical effect of the intermediate dielectric layer is still poorly understood. There are only a few reports in the literature about the experimental evidence of such plasmon resonance [20]. The discrepancies between theoretical calculation and experimental results are quite evident.

Under such circumstances, the major challenge in the study of multilayer SPR biosensors is to determine the best way to improve the performance of the system and to collect first-hand experimental evidence to confirm the theoretical analyses. The major goal of this research is to determine the effects of the intermediate dielectric film materials in a multilayer configuration.

2. Effects of intermediate dielectric layers on SPR

The SPR curve of reflectivity R vs. incident angle θ of a multilayer SPR configuration can be calculated or simulated based on the theoretical analysis of the Fresnel reflection. Various computer programs have been developed to calculate the resonance behavior of the multi-phase configuration. Among those accessible in open literature is a calculation program developed by the University of California at Irvine based on the article by Hansen [24], which has been widely used and has proved to be a simple, powerful and trustworthy simulation program. However, the original program was given in the form of a macro for the software program IGOR PRO (Wavemetric's, Inc.). We transplanted it into a MATLAB environment, making it more user friendly and enabling it to be operated on any PC computer under MATLAB. To calculate the resonance curve, the refractive indices n_i and thicknesses d_i of each layer need to be known. The simulation program used in this work in the form of MATLAB is available upon request. With the help of this program, the SPR behaviors of various complicated configurations can be theoretically predicted.

To analyze the effects of the intermediate dielectric layers on the SPR curves, a simplified model as shown in Fig. 2 was used, where the prism with refractive index of n_1 is represented as a semi-infinite medium 1, and the bio-analyte with refractive index n_2 is counted as a semi-infinite medium 2. The intermediate dielectric layer with refractive index n_i and thickness d_i, and the metal film with refractive index of n_m and thickness d_m are sandwiched between the semi-infinite medium 1 and medium 2. Using this simplified model the resonance curves of multilayer SPR configurations with various refractive indices and thicknesses of the intermediate dielectric layers can be calculated.

Fig. 3 shows that the resonance curves of a multilayer SPR configuration with the refractive index of the prism is 1.5163 RIU and the refractive indices of the intermediate dielectric layers vary from 1.1 to 2.8 RIU, while the thickness of the dielectric layers is fixed at 500 nm and the thickness of the gold metal film is fixed at 45 nm. The refractive index of the bio-analyte is taken as 1.0 RIU. It can be seen from the figure that the resonant angles are only slightly affected by the intermediate dielectric layers in all cases, while the widths of the resonance curves are strongly affected by the refractive indices of the dielectric layers. When the refractive index of the intermediate dielectric layer varied between 1.5 and 2.5 RIU, the variation of the resonance width was not quite evident. However, when the refractive indices of the dielectric layers decreased to 1.2 and 1.1 RIU, the resonance width decreases markedly. The low refractive index of the intermediate dielectric layer around 1.0–1.2 RIU results in a more or less symmetric deployment of refractive index on the opposite side of the metal film. It is widely recognized that a symmetric SPR

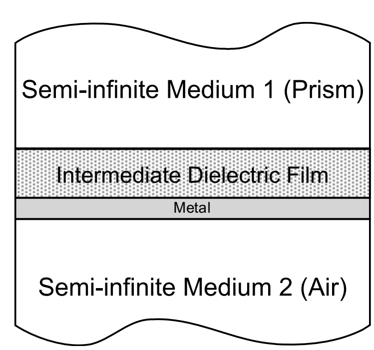

Fig. 2. Calculation model of a multilayer SPR configuration.

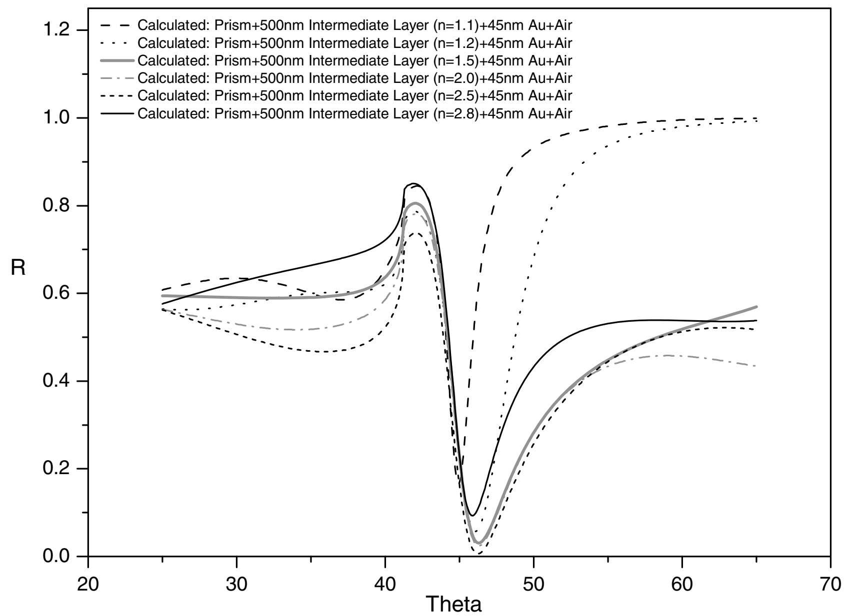

Fig. 3. Resonance curves of the multilayer SPR configuration.

configuration is characterized by a long-range SPR with a very sharp SPR curve [17,20]. Our results are in good agreement with the reports in the open literature. Surprisingly, the very asymmetric deployment of the intermediate dielectric layer with a very high refractive index of 2.8 also results in a sharp SPR curve, as shown in Fig. 3. A sharp SPR resonance curve for an asymmetric configuration was predicted by Zervas [25]. Our results also confirmed the prediction.

Figs. 4–6 are the resonance curves of the multilayer SPR configurations with various dielectric thicknesses ranging from 100 to 800 nm at fixed refractive indices of 1.2, 1.5 and 2.83 (the refractive index of TiO_2 is 2.83), respectively. The refractive index of the prism is 1.5163 RIU. The thickness of the gold metal film is still fixed at 45 nm. It can be seen from Figs. 4 and 6 that when the refractive index of the dielectric layer is different from that of the prism, the thickness dependence of the SPR behavior of the multilayer SPR configuration is quite evident. Sharper SPR curves can be achieved at reasonable thicknesses of the dielectric films. The optimum thicknesses are 300–500 nm for the dielectric film with a refractive index of 1.2 RIU

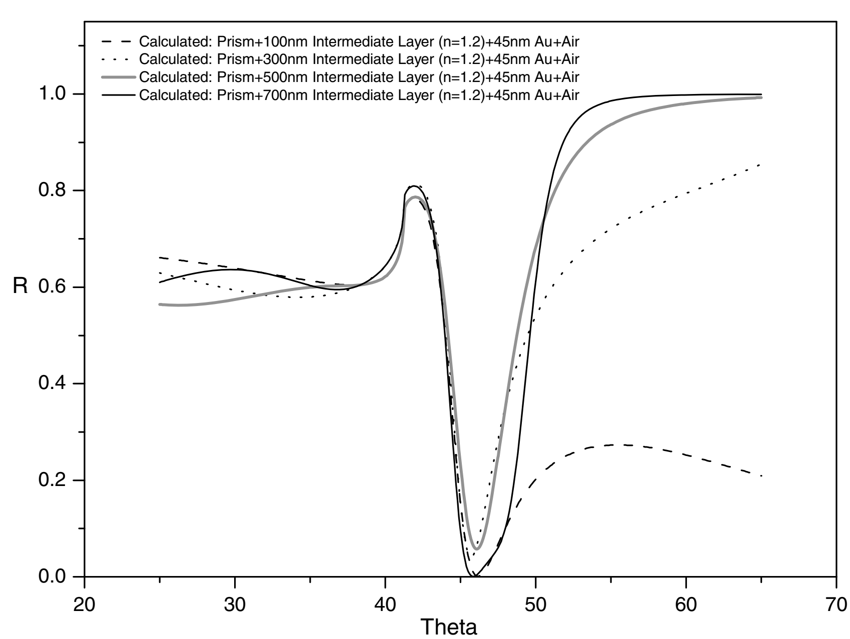

Fig. 4. Resonance curves of the multilayer SPR configuration with various intermediate thicknesses ranging from 100 to 700 nm at a fixed refractive index of 1.2.

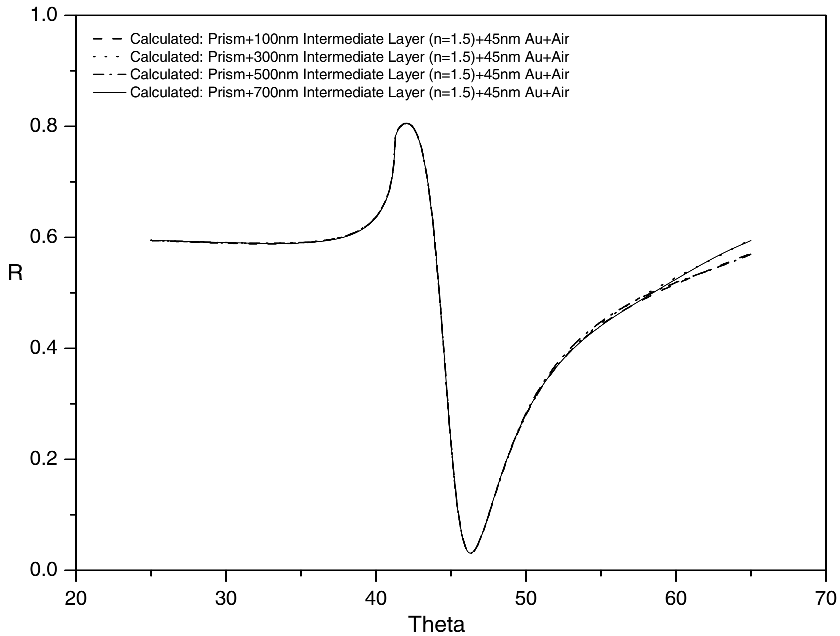

Fig. 5. Resonance curves of the multilayer SPR configuration with various intermediate thicknesses ranging from 100 to 700 nm at a fixed refractive index of 1.5.

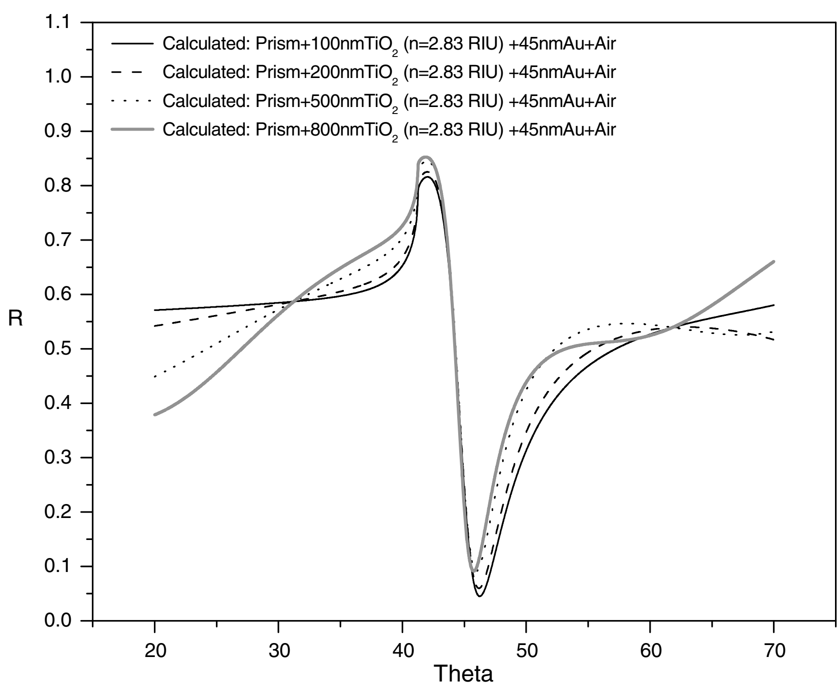

Fig. 6. Resonance curves of the multilayer SPR configuration with various intermediate thicknesses ranging from 100 to 800 nm at a fixed refractive index of 2.83 (TiO_2).

and 500–800 nm for the film with a refractive index of 2.8 RIU. However, when the refractive index of the dielectric film is close to that of the prism (1.5 RIU in our case), the thickness dependence of the resonance is negligible; the SPR curves of the multilayer configuration with various thicknesses of the dielectric film are almost the same, as shown in Fig. 5. It can be easily understood that in such a case the dielectric film can be considered as an extension of the prism. However, the thickness dependence of the resonance curves with refractive indices far from that of the prism seems rather complicated; some optical phenomena other than the SPR might be superimposed to the SPR, especially at the high angle side of the resonance.

It should be also noted here that the thickness of the metal film also strongly affects the resonance behavior of the multilayer SPR configuration. The resonance behavior can be further optimized by changing the metal film thickness in each combination of refractive index and thickness of the dielectric film.

3. Experimental

3.1. Experimental set-up

A home-constructed apparatus of SPR, based on Kretschmann geometry, was built for this study. An outline of the experimental arrangement is given in Fig. 7.

The set-up consists of a green laser operating at 543.5 nm for the excitation source of surface plasmon. The power stability of the laser is better than ±2.5% over 8 h, with noise below 1%. To enhance the quality of the laser beam, a spatial filter is used to "clean up" the laser beam to a Gaussian profile. The diameter of the light beam is around 0.8 mm, the beam divergence is better than 0.86 mrad. The *p*-polarization light mode is achieved by passing the laser beam through a polarizer.

A half cylindrical prism with a refractive index of 1.5163 was used throughout this work. In this case, if the incident beam hits the prism along the normal direction of the round surface, then the incident beam remains normal throughout the rotation of the prism. Therefore, the coupling spot at the metal film is stationary and the measurement is more consistent because of the fixed measuring point. In addition, the use of a cylindrical coupler facilitates the positioning of the rotation axis and significantly reduces the corresponding errors that are easily introduced by deviation from the rotation axis. It also allows a much wider range of angular scanning with a relative simple design and operation.

Thin film samples are prepared on a glass substrate with a refractive index of 1.515 and attached to the prism by applying index-matching oil in between. The prism/thin film sample complex is mounted on a self-made $\theta - 2\theta$ goniometer. The goniometer includes two high-resolution rotational stages (Edmond Inc.) that are connected together such that their axes of rotation are collinear. An Astral AP30 silicon photodiode is assembled onto the 2θ stage to detect the reflected beam from the sample.

3.2. Sample preparation

Generally, it would be better to deposit the multilayer Kretschmann configuration directly onto the prism surface in order to achieve the lowest insertion loss and highest sensitivity. However, from the practical application point of view, it is highly desirable to implement a separate test sample into the system and keep the prism intact. Since the glass prism is a key component of the test system, the quality and mounting condition of the prism are very sensitive to the test results.

Separate test samples with multilayer Kretschmann configuration deposited onto a glass substrate are easy to prepare and easy to use. Glass substrate samples are cheap and disposable. It would be better to use glass substrates with the same refractive index as the prism and keep the sample substrate in close contact with the prism. To minimize the mismatch effect of the air gap between the glass substrate and the prism, matching oil with the same refractive index as the glass substrate and the prism is used to mount the test samples into the test system. When high temperature treatment is involved in the sample preparation process, high silica glass substrates are good candidates for the applications. In this work, high silica glass of size $12 \times 12 \times 0.5\ mm^3$ was used as substrates. Both sides of the substrates were well polished.

3.2.1. Deposition of dielectric films

The major goal of this research was to survey the dielectric film materials in a multilayer SPR configuration. In order to obtain revelatory information from such a study, it would be better to make a systematic evaluation on a group of dielectric materials with different dielectric and optic behaviors. In this work 10 dielectric films were investigated, of which five were simple oxide/fluorides and five were complex oxides. The refractive indices (at about 550 nm) of the 10 dielectric films covered very wide range, from 1.19 to 2.80, as given in Tables 1 and 2. To manipulate the porosity of SiO_2 films it is possible to fine tune the refractive index of the SiO_2 film within the range of 1.19–1.43. To manipulate the PZT/SiO_2 ratio, it is possible to tune the refractive index of PZTS film in the range of 1.48–2.39.

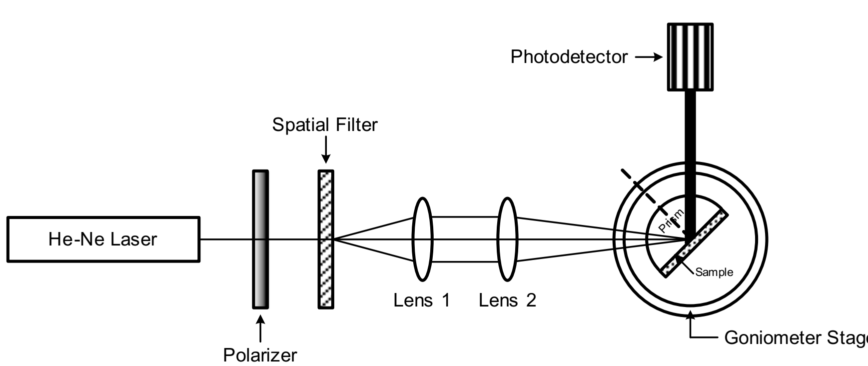

Fig. 7. Schematic of the prism-coupled Kretschmann set-up constructed for this work.

The dielectric films of MgO, MgF_2 and TiO_2 were deposited onto well-polished silica glass substrates by electron beam evaporation. Sol–gel and spin coating wet chemistry technology were used to prepare dense and porous SiO_2, PZT ($Pb(Zr_{0.5}Ti_{0.5})O_3$), PLZT ($(Pb_{0.94}La_{0.06})(Zr_{0.5}Ti_{0.5})O_3$), PZTS (PZT–$SiO_2$), BSZT ($(Ba_{0.7}Sr_{0.3})(Zr_{0.7}Ti_{0.3})O_3$) and LNO ($LaNiO_3$) films. The details of the deposition techniques of various dielectric films can be found elsewhere.

3.2.2. Deposition of the metal film

As mentioned above, gold is acknowledged to be the best metal for SPR. In this work, standard 45 nm gold was used in all the experiments.

The gold film was deposited either directly onto the substrates for the single-layer SPR configuration or onto the pre-deposited dielectric layer for the multilayer SPR configuration. In this work, an E-beam evaporator (Edwards, Auto306) was used to deposit the gold film. The vacuum of the deposition chamber was 5×10^{-6} Torr. The deposition rate of the gold film was about 1 Å s^{-1}.

3.3. Experimental results

In order to examine the effect of intermediate dielectric films on SPR for biosensor applications, surface plasmon resonant curves of multilayer configuration with various intermediate dielectric films were taken and compared with that of the basic SPR configuration without the intermediate dielectric layer.

3.3.1. Reference R–θ curve for the basic SPR configuration

Fig. 8 shows the experimental result of the R–θ curve of the prism/gold/air basic SPR configuration. The minimum point of the reflectance is corresponding to the SPR angle $\theta_R = 46.0°$ and the minimum reflectance value R_{min} is 0.0517. This R–θ curve will be used as the basic reference state against which are compared the results of various multilayer configurations using various intermediate dielectric layers. In order to compare the resonance feature of the surface plasmon with various configurations, the difference in the incident angles $\Delta\theta$ of the resonance curve cutting with $R_{min} + 0.2$ are defined as the width of the resonance curve and used as a reference parameter against which to compare the resonance behavior of various configurations. The experimental result of $\Delta\theta$ of the basic SPR configuration is 5.33°.

3.3.2. Resonance features of multilayer SPR configurations

Various dielectric materials listed in Tables 1 and 2 have been evaluated as intermediate dielectric layers in the multilayer SPR geometry. Three major features of the SPR resonance curve are also calculated by using a MATLAB simulation program. Table 3 lists the experimental and calculated results of 10 tested materials.

Table 1
Refractive indices of simple oxides and fluoride

	Porous SiO_2	MgF_2	Dense SiO_2	MgO	TiO_2
n	1.19–1.43	1.3844	1.4316	1.741	2.829

Table 2
Refractive indices of complex oxides

	PZT	PLZT	PZTS	BSZT	LNO
n	2.40	2.52	1.48–2.39	2.11	–

It can be seen from the results that the experimental resonance angle θ_R in all cases was around $46.0 \pm 0.3°$, which is quite close to the calculated results within experimental errors. The intermediate dielectric layer has no strong effect on the resonance position of the SPR system.

The minimum reflectance R_{min} of all the experimental results was very low, in the range of 0.03–0.07. The intermediate dielectric layer also had no strong effect on the minimum reflectance and was in the same range as the calculated results.

The width of the SPR curves was affected by the refractive index and thickness of the intermediate dielectric film. The changing of the resonant width $\Delta\theta$ of experimental results followed the same trend as the calculation results. From the calculation results, a sharpening effect on the resonance behavior of the intermediate dielectric layer of such materials as MgF_2, TiO_2, dense and porous SiO_2 and PLZT can be expected. Of these materials, the porous silica, with a very low refractive index, forming a symmetric configuration, and TiO_2, with a very high refractive index, forming a very asymmetric configuration, are the most elaborate. The width of the SPR curves obtained from the experimental results is in general higher than the calculation results, except for the high refractive index films of TiO_2 and PLZT. The measurements on the high refractive index films are rather scattered. Further studies to obtain more elaborate results are needed. However, it is clear that they follow the same trend as the calculated ones. In Table 3, no calculated results are presented for PZT–SiO_2 and LNO film as no reliable refractive indices of the samples were available.

Some examples of the SPR curves are given and discussed in the following sections.

3.3.3. Examples of the SPR resonance curve with various intermediate dielectric films

Fig. 9 shows the experimental R–θ curve of the prism/MgF_2/gold/air configuration with a 100 nm MgF_2 intermediate layer. MgF_2 is widely used as a coating film for optical lenses and components; hence, it was used as an intermediate dielectric layer in the multilayer SPR studies. Both theoretical analysis and experimental studies have been conducted elsewhere [17,20]. In this work, MgF_2 intermediate dielectric layers with different thicknesses were studied experimentally.

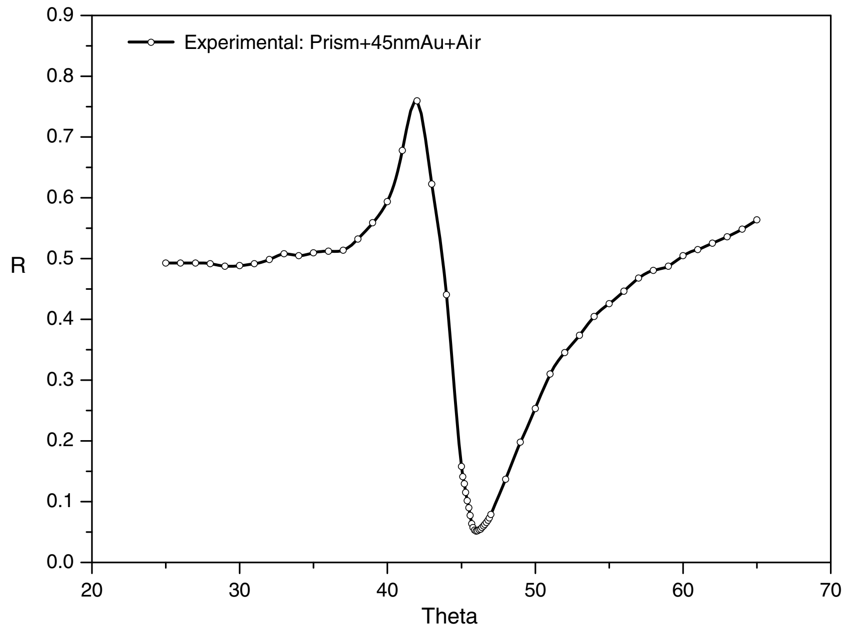

Fig. 8. Experimental R–θ curve of basic SPR of prism/gold/air configuration.

Table 3
Experimental and calculated results of SPR curves

#	Sample configuration	θ_R°		R_{min}		$\Delta\theta$°	
		Exp.	Calc.	Exp.	Calc.	Exp.	Calc.
1	Prism/45 nm Au/air (as reference)	46.0	46.30	0.0517	0.0307	5.33	4.18
2	Prism/500 nm MgF_2/45 nm Au/air	46.0	46.23	0.0335	0.0294	4.21	3.99
3	Prism/500 nm MgO/45 nm Au/air	46.1	46.25	0.0412	0.0283	5.70	4.19
4	Prism/500 nm TiO_2/45 nm Au/air	45.7	45.97	0.0556	0.0911	3.12	3.21
5	Prism/500 nm denseSiO_2/45 nm Au/air	46.1	46.27	0.0452	0.0318	5.75	3.99
6	Prism/500 nm porousSiO_2/45 nm Au/air	46.3	46.00	0.0436	0.0723	3.52	2.43
7	Prism/500 nm PZT/45 nm Au/air	46.1	46.23	0.0386	0.0456	5.98	3.78
8	Prism/500 nm PLZT/45 nm Au/air	46.2	46.19	0.0360	0.0027	4.01	4.50
9	Prism/500 nm PZT–SiO_2/45 nm Au/air	46.0	–	0.0679	–	7.44	–
10	Prism/500 nm BSZT/45 nm Au/air	46.1	46.10	0.0715	0.0103	5.59	4.24
11	Prism/500 nm LNO/45 nm Au/air	46.2	–	0.0515	–	4.92	–

The basic R–θ curve of prism/gold/air is also plotted in Fig. 9 for reference. Comparing the experimental results of prism/MgF_2/gold/air configuration with those of the basic SPR with gold only (Fig. 8), it can be seen that the incorporation of a 100 nm MgF_2 intermediate dielectric layer has no significant effect on the resonance angle θ_R and the reflectance minimum R_{min}, while the width of the resonant curve $\Delta\theta$ is reduced to 4.63, compared to the 5.33 of the basic SPR. A sharper resonance curve means a better resolution, hence a higher sensing performance for biosensing applications. This result is consistent with the previous research on the MgF_2-based multilayer SPR.

Fig. 10 is the experimental R–θ curve of the prism/MgF_2/gold/air configuration with a 500 nm MgF_2 intermediate layer. It is quite evident from the figure that the experimental result of 500 nm MgF_2 is almost identical to that in the 100 nm case. The thickness dependence of the MgF_2 intermediate layer has no significant effect on the SPR resonance. It can be seen from the experimental results that the presence of an MgF_2 intermediate dielectric layer effectively reduces the SPR resonant width.

Figs. 11 and 12 present the experimental R–θ curves of the multilayer SPR configuration with dense and porous silica intermediate layers, respectively. The basic R–θ curve of the configuration without SiO_2 intermediate layer is also plotted in the figures for comparison. The refractive index n of the dense silica film is 1.4316, while that of porous silica film is 1.1895 as measured from Filmtick F-20. The thickness of the films is 500 nm.

The SPR resonant angle θ_R, minimum reflectance R_{min} and resonant width $\Delta\theta$ of the sample with dense silica films are not significantly different from those of the basic SPR configuration without silica film. Since the refractive index of the dense silica film is quite close to that of the silica glass substrate, this result can be easily understood. However, although the SPR resonant angle θ_R and minimum

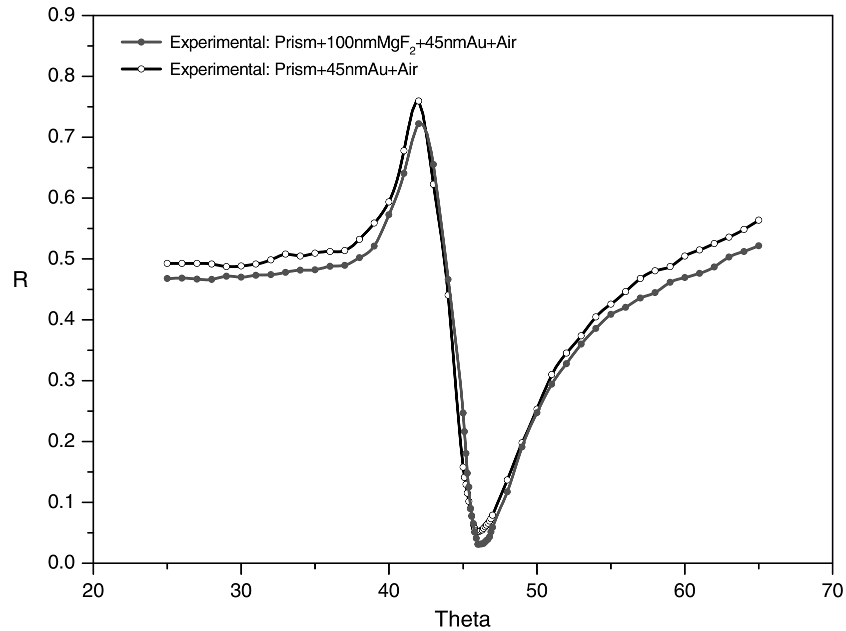

Fig. 9. Experimental R–θ curve of the prism/MgF_2/gold/air configuration (100 nm MgF_2).

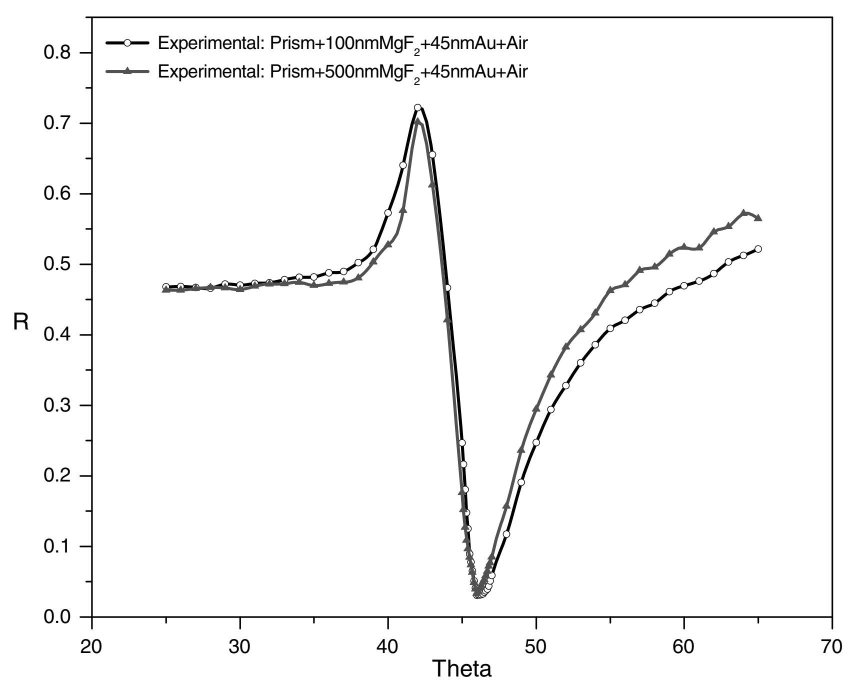

Fig. 10. Experimental R–θ curves of the prism/MgF_2/gold/air configuration with different thickness (100 and 500 nm MgF_2).

reflectance R_{min} of the sample with porous silica film are almost the same as for the basic SPR configuration, the width of the resonant curve $\Delta\theta$ is lower, which means a better sensing performance.

The shape of the R–θ curve of the multilayer SPR with a porous silica intermediate dielectric layer is different from most of the other experimental R–θ curves. The maximum reflectance value at a low incident angle is greatly suppressed, at only 0.64, while in most of other cases, the corresponding maximum reflectance is in the range 0.7–0.8. In addition, the reflectance at high incident angles beyond the SPR angle θ_R increases rapidly and keeping at the high level of 0.7–0.8. Both effects can be accounted for by the porous structure of the silica films. The porosity of the porous silica film is around 53% as calculated from the refractive index. The pore size distribution of the porous silica film is very wide, covering the range from tens to hundreds of nanometers. The light scattering of the porous structure

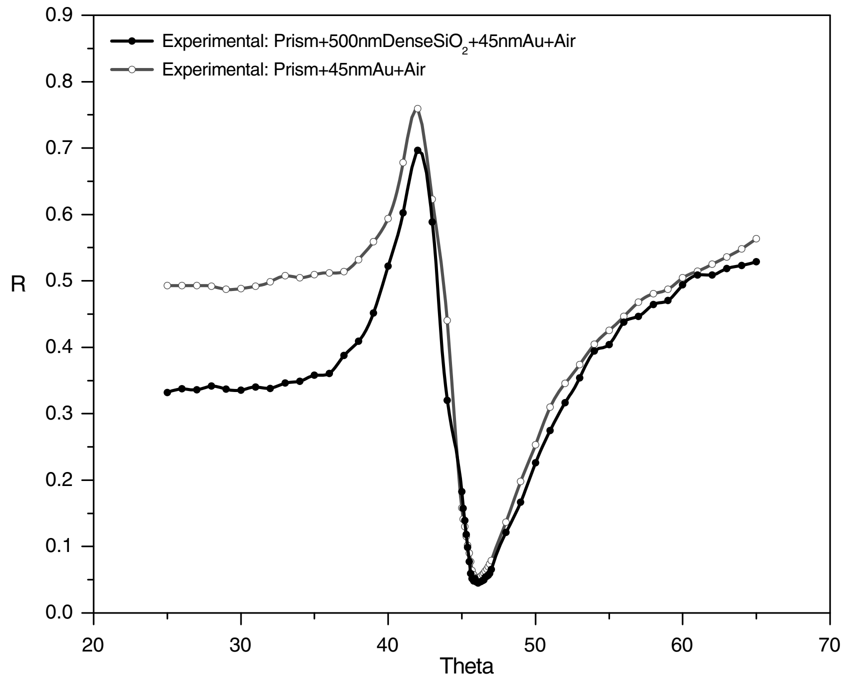

Fig. 11. Experimental R–θ curve of the multilayer SPR configuration with a dense silica intermediate layer.

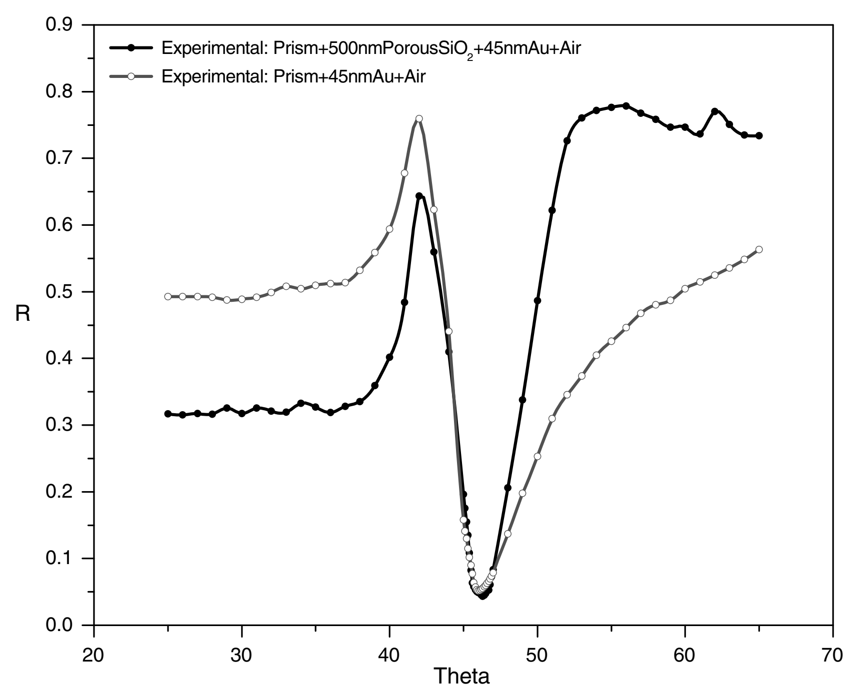

Fig. 12. Experimental R–θ curve of the multilayer SPR configuration with a porous silica intermediate layer.

is very high. When the incident angle is low, the scattering loss of the light beam is high, causing a lower reflectance. When the incident angle is high, the scattered light collected by the detector along the direction of the reflection beam will also be high, therefore resulting in a high reflectance.

Fig. 13 shows the experimental R–θ curve of the multilayer SPR configuration with PLZT [$(Pb_{0.94}La_{0.06})(Zr_{0.5}$-$Ti_{0.5})O_3$] as the intermediate dielectric layer. It is well known from studies of the PZT ceramic family that doping with La^{3+} to substitute part of the Pb^{2+} in $Pb(Zr,Ti)O_3$ can improve the optical behavior of the ceramic. It was therefore interesting to see whether the PLZT intermediate dielectric layer would be able to improve the SPR performance. PLZT film was prepared by sol–gel synthesis and the spin coating process. The refractive index n of the PLZT

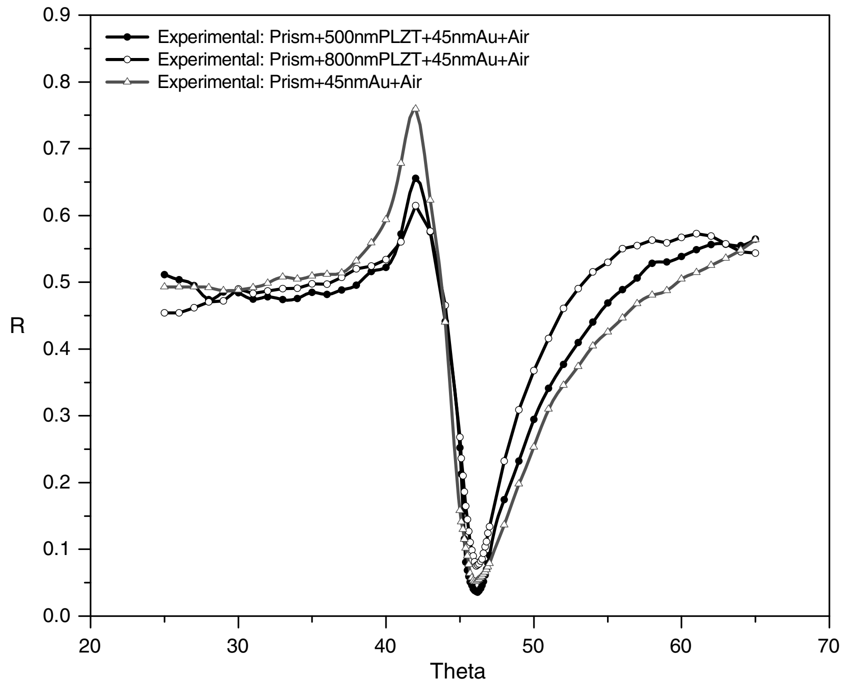

Fig. 13. Experimental R–θ curves of the multilayer SPR configuration with PLZT as the intermediate dielectric layer.

film was 2.52, which is higher than that of the pure PZT film due to the chemical doping of lanthanum. The thicknesses of film were around 500 and 800 nm. The SPR resonance width $\Delta\theta$ was 4.01 and 3.55, respectively, for PLZT thicknesses of 500 and 800 nm. The results are much improved over the PZT case as well as the basic SPR configuration.

4. Summary

It is concluded from the above investigations that the intermediate dielectric film in a multilayer SPR configuration has no significant effect on the SPR resonant angle and minimum reflectance at the resonance point. Intermediate dielectric films such as MgF_2, TiO_2, porous silica and PLZT are able to reduce the width of the SPR resonant curve, resulting in a sharper resonant curve. Better performances in sensitivity and resolution of the multilayer SPR biosensor with these intermediate dielectric films can be expected. From the above investigation it can also be seen that the difference in the refractive index between the intermediate dielectric film and the glass substrate/prism plays a major role in the resonance behavior of the multilayer SPR configuration. To achieve a higher performance of the SPR for biosensor applications, intermediate dielectric films with either low or high refractive index are preferable. The experimental results were confirmed and found to be in good agreement with the calculated ones.

Based on the experimental study on the effect of intermediate dielectric layer, it is important to note here that the microstructure and lattice defects of the intermediate dielectric films in a multilayer surface plasmon configuration could have a profound effect on the SPR behavior. So far, such an effect has not been taken into account in the theoretical analysis and simulation calculation of the SPR phenomena. In almost all the analyses and calculations, only the refractive index and thickness of the intermediate dielectric film have been involved. The atomistic nature and lattice nature of the films as well as their microstructures and defects have also been ignored. This situation is obviously unsatisfactory, and should be improved in future investigations. The lattice and microstructure nature and defects of the dielectric films are considered to be responsible for the higher resonance width obtained from experiments in comparison with the theoretical calculation.

References

[1] Nylander C, Liedberg B, Lind T. Gas detection by means of surface plasmon resonance. Sensor Actuator 1982;3:79–88.
[2] Liedberg B, Nylander C, Lundstrom I. Surface plasmons resonance for gas detection and biosensing. Sensor Actuator 1983;4:299–304.
[3] Liedberg B, Nylander C, Lundstrom I. Biosensing with surface plasmon resonance – how it all started. Biosens Bioelectron 1995;10:i–ix.
[4] Gizeli E, Lowe CR. Biomolecular sensors. Taylor & Francis; 2002, [chapter 9].
[5] Huber A, Demartis S, Neri D. The use of biosensor technology for the engineering of antibodies and enzymes. J Mol Recognit 1999;12:198–216.
[6] Malmqvist M. Surface plasmon resonance for detection and measurement of antibody–antigen affinity and kinetics. Curr Opin Immunol 1993;5:282–6.
[7] Rahn JR, Hallock RB. Antibody binding to antigen-coated substrates studied with surface plasmon oscillations. Langmuir 1995;11:650–4.
[8] Adamczyk M, Moore JA, Yu Z. Application of surface plasmon resonance towards studies of low-molecular-weight antigen–antibody binding interactions. Methods 2000;20:319–28.
[9] Fujii E, Nakamura K, Sasaki SI, Citterio D, Kurihara K, Suzuki K. Application of the absorption-based surface plasmon resonance

principle to the determination of glucose using an enzyme reaction. Instrum Sci Technol 2003;31:343–56.
[10] Merwe PA, Barclay AN. Analysis of cell–adhesion molecule interactions using surface plasmon resonance. Curr Opin Immunol 1996;8:257–61.
[11] Nilsson P, Persson B, Larsson A, Uhlen M, Nygren P. Detection of mutations in PCR products from clinical samples by surface plasmon resonance. J Mol Recognit 1997;10:7–17.
[12] Slepak VZ. Application of surface plasmon resonance for analysis of protein–protein interactions in the G protein-mediated signal transduction pathway. J Mol Recognit 2000;13:20–6.
[13] Myszka DG, Rich RL. Implementing surface plasmon resonance biosensors in drug discovery. Pharm Sci Tech Today 2000;3:310–7.
[14] Homola J, Yee SS, Gauglitz G. Surface plasmon resonance sensors: review. Sensor Actuator B 1999;54:3–15.
[15] Raether H. Surface plasmons on smooth and rough surfaces and on gratings. Springer; 1988.
[16] Kretschmann E, Raether H. Radiative decay of non-radiative surface plasmons excited by light. Z Naturforsch 1968;23A:2135–6.
[17] Matsubara K, Kawata S, Minami S. Multilayer system for a high-precision surface plasmon resonance sensor. Opt Lett 1990;15:75–7.
[18] Lin CW, Chen KP, Hsiao CN, Lin S, Lee CK. Design and fabrication of an alternating dielectric multilayer device for surface plasmon resonance sensor. Sensor Actuator B 2006;113:169–76.
[19] Kessler MA, Hall EAH. Multilayered structures exhibiting long-range surface exciton resonance. Thin Solid Films 1996;272:161–9.
[20] Nenninger GG, Tobiska P, Homola J, Yee SS. Long-range surface plasmons for high-resolution surface plasmon resonance sensors. Sensor Actuator B 2001;74:145–51.
[21] Van Gent J, Lambeck PV, Kreuwel HJM, Gerritsma GJ, Sudholter EJR, Reinhoudt DN, et al. Optimization of a chemooptical surface plasmon resonance based sensor. Appl Opt 1990;29:2843–9.
[22] Brink G, Sigl H, Sackmann E. Near-infrared surface plasmon resonance in silicon-based sensor: new opportunities in sensitive detection of biomolecules from aqueous solutions by applying microstep for discriminating specific and non-specific binding. Sensor Actuator B 1995;25:756–61.
[23] Kooyman RPH, Kolkman H, Van Gent J, Greve J. Surface plasmon resonance immunosensors: sensitivity considerations. Anal Chim Acta 1988;213:35–45.
[24] Hansen WN. Electric fields produced by the propagation of plane coherent electromagnetic radiation in a stratified medium. J Opt Soc Am 1968;58:380–90.
[25] Zervas MN. Surface plasmon-polariton waves guided by thin metal films. Opt Lett 1991;16:720–2.